Received: 21 March 2023 | Revised: 17 May 2023 | Accepted: 14 July 2023

DOI: 10.1002/elan.202300087

RESEARCH ARTICLE

ELECTROANALYSIS

In situ electrochemical monitoring of signaling transduction in plants. Implications on phylogenetic aspects of defense response

Antonio Doménech-Carbó[1] | **Daiane Dias**[2] | **Josefa Prieto-Mossi**[3] | **Noemí Montoya**[4]

[1]Departament de Química analítca, Universitat de València, Burjassot (València) Spain

[2]Laboratório de Eletro-Espectro Analítica (LEEA), Escola de Química e Alimentos, Universidade Federal do Rio Grande, Rio Grande, Brazil

[3]Jardí Botànic - ICBiBE Universitat de València., València, Spain

[4]Facultad de Ciencias de la Salud, Universidad Internacional de la Rioja. UNIR, Logroño, La Rioja, Spain

Correspondence
Antonio Doménech-Carbó, Departament de Química analítca, Universitat de València, Dr. Moliner, 50, 46100 Burjassot (València) Spain.
Email: antonio.domenech@uv.es

Funding information
European Union

Abstract

In situ recording of the voltammetric response of leaves of several Asparagales, Caryophyllales, and Saxifragales plants at platinum and graphite microelectrodes is described. These provide information on the temporal evolution of H_2O_2 production and electroactive defense compounds (salicylic and jasmonic acids) associated with the stress generated by electrode insertion. Comparison of voltammetric data in the absence and presence of ROS generation revealed significant differences in the kinetics of the plant response. Reported data suggest that signaling pathway changes could be associated with the phylogenetic divergence between monocots and eudicots and the subsequent separation of the Caryophyllales from other eudicots.

KEYWORDS
defense signaling, electrochemistry, *in situ*, phylogeny, ROS

1 | INTRODUCTION

Studies on plant physiology based on electrochemical techniques involve a variety of issues, including recognition of plant growth regulators [1], analysis of growth conditions [2], and uptake of biocomponents [3]. Plant defense responses (both constitutive and induced) against different types of stress (physical, chemical and biological) involve signal transduction by means of signaling compounds [4, 5] and the release of defense species, including reactive oxygen species (ROS) [6, 7]. Jasmonic acid (JA) and salicylic acid (SA) have been characterized as important signaling compounds [8, 9]. The former acts as a mediator in many plant defense responses [10–12], while the second appears to operate independently [12] and even in contraposition to other signaling pathways [13–15]. These features have an evolutionary dimension [16] that can be formulated in terms of i) what is the role of the defense response in plant evolution?, and ii) what is the role of the different defensive responses in the evolution of the different taxonomic groups? These questions can be formulated within a complex evolutionary scenario where herbivory has promoted a change in plant metabolism from growth-oriented to

defense-oriented [17] so that the phylogeny and plants and insects should be closely related [18–21].

Accordingly, the regulation pathways of the signaling compounds can offer issues on evolutionary aspects on treating their relation with wound signals, such as ROS [22–24], and influence plant development [25–27]. The investigation of these matters involves the monitoring of plant responses against stress. Apart from the intrinsic difficulty of *in vivo* or *in situ* analysis, monitoring defense pathways is considerably complicated by the coexistence of an enormous variety of plant components in turn participating in complex metabolic cycles [28–30]. For this reason, although there are different possibilities for electrochemical studying ROS [31–34], *in situ* electrochemical monitoring of defense pathways is mainly confined to H_2O_2 production [35, 36].

In this context, previous works revealed the suitability of electrochemical techniques to acquire information on the role of gynodioecy in adaptation to stress [37], response to herbivory [38] and chemotaxonomic and phylogenetic information [39–41]. More recently, an *in situ* study on the kinetics of the response of *Aloe vera* L. to mechanical stress, suggested that the signaling pathways of JA and SA operate independently with different kinetics [42]. These results also suggested the possibility of extracting phylogenetic information in terms of the coupling/decoupling relationships between the different defense pathways. Operationally, this can be formulated in terms of at least two questions: if the different signaling pathways appeared independently in different stages of plant evolution, or if these pathways appeared similarly in different taxonomic groups. Several other phylogenetic factors (plant growth and harvesting conditions, environmental constraints, ...) are influential on the individual plant defense response so the reported study must be taken as a methodological approach potentially interesting to provide information of phylogenetic meaning.

Here, we report an *in situ* voltammetric and scanning electrochemical microscopy (SECM) study of the response to mechanical stress of nine plants of three families. These species were selected based on: i) their succulent character prompting stable microelectrode insertion; ii) growth in the same environmental conditions (Burjassot, Valencia University campus); iii) ascription to clearly separated taxa [43] whose phylogeny is to some extent matter of speculation [44–47]. Our selected plants include three monocots (*Aloe vera* (L.) Burm.f., *Asphodelus fistulosus* L., and *Bulbine frutescens* (L.) Willd., order Asparagales) and six core eudicots species, these last divided into two orders, Saxifragales (*Crassula ovata* Druce, *Sedum sediforme* (Jacq.) Pau, and *Graptopetalus paraguayense* (N.E.Br.) E. Walther) and Caryophyllales (*Aptenia cordifolia* (L.f.) Schwantes, *Delosperma cooperi* (Hook.f.) L.Bolus, and *Faucaria tigrina* (Haw.) Schwantes).

Our study exploits the capability for electrochemically generating ROS [48–50] including the monitoring of the time evolution of the concentrations of H_2O_2, JA and SA. The former was monitored using platinum as a working electrode because of its high interaction with H_2O_2 [35, 36], while JA and SA were tested using graphite microelectrodes. Here, a kinetic model aimed to acquire mechanistic information is developed. Voltammetric data are complemented by *in situ* SECM monitoring of the activation/deactivation of the signaling pathways associated to the electrochemical generation of ROS using the redox competition mode [51]. Ultimately, the study was aimed to establish: i) if there is a common defense pathway operating in the plants of the same family, ii) if there are family-characteristic defense pathways, and, iii) if these differences, if existing, can be correlated with their phylogenetic position.

2 | EXPERIMENTAL

Leaves of the studied plants were taken from healthy plants existing in the gardens of the University of Valencia campus in Burjassot and in Botanical Garden of the University of Valencia. The electrochemical measurements were performed immediately after the separation of the leaves from the plant. The plant specimens were harvested during the maturity step of the plants. Platinum (CHI107, diameter 25 μm) and graphite (Staedtler, 0.5 mm diameter) were alternatively used as a working electrode, being accompanied with platinum auxiliary and pseudoreference microelectrodes of diameter 100 μm (CHI108) connected to a CH 720c potentiostat. The mechanical stress was produced by the insertion of the electrodes which disrupt the epithelial and sub-epithelial region of leaves. The electrodes were inserted perpendicularly into the plant leaves as illustrated in the image added as an inset in Figure 1. The electrodes were inserted perpendicularly to the leaf surface at a depth of 2 mm and fixed to supports with the help of clamps. The positions of the electrodes were selected to form a triangle with separations of 2 mm between them. Voltammetric measurements were initiated just after the insertion of the electrodes marking the 'time zero' for kinetic calculations. Voltammetric measurements were carried out at room temperature ($25 \pm 1\,^{\circ}C$) under uniform relative humidity ($60 \pm 10\,\%$) and illumination

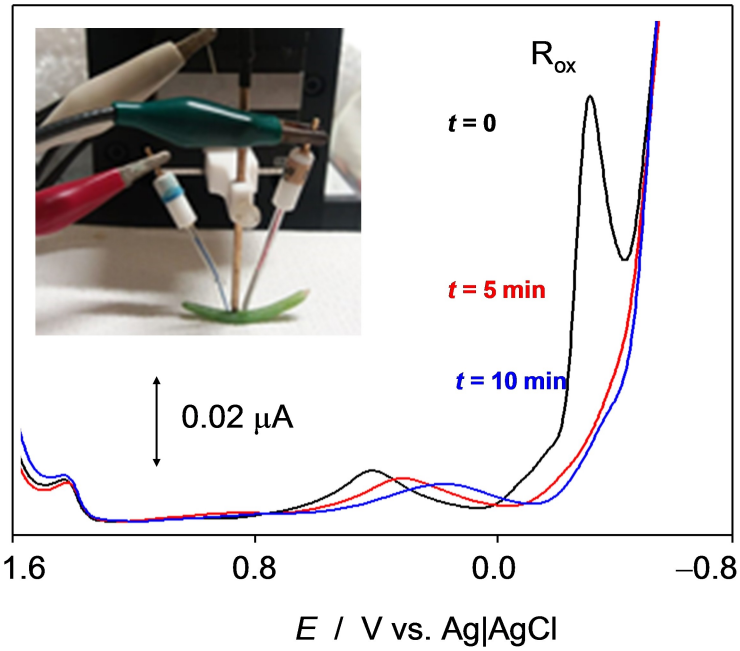

FIGURE 1 SWVs at platinum microelectrode inserted into a leaf of *Faucaria tigrina* at different times after electrode insertion. Potential scan initiated at 1.6 V vs. Ag/AgCl in the negative direction; potential step increment 4 mV, square wave amplitude 25 mV; frequency 10 Hz. Inset: Photographic image of the experimental arrangement used for *Delosperma cooperi*.

(white LED lamp 17 w, 1600 lumen). Square wave voltammetry (SWV) was routinely used as a detection mode. Prior to the electrochemical series of runs, the electrodes were immersed for 5 min in 1 M H_2SO_4 and subsequently rinsed with water. The potentials were calibrated vs. Ag/AgCl (3 M NaCl) using a 1.0 mM $K_3Fe(CN)_6$ plus 1.0 mM $K_4Fe(CN)_6$ solution in aqueous 0.10 M KCl.

SECM experiments were carried out on thin films (surface area ca. 0.5 mm^2) of the subcuticular region of the leaves extracted with a scalpel and deposited over a graphite paste (50% wt graphite plus 50% wt nujol oil) bed covering a Pt substrate electrode. A Pt microelectrode tip (CH 49, diameter 20 μm) was used. The distance between the tip and the substrate was of the order of the tip electrode radius and the tip scanning rate over the substrate was 20 $\mu m\,s^{-1}$. The electrolyte solution consisted of air-saturated 2.5 mM $K_3Fe(CN)_6$ plus 2.5 mM $K_4Fe(CN)_6$ phosphate buffer at pH 7.4.

3 | RESULTS AND DISCUSSION

3.1 | Voltammetric pattern

Figure 1 superimposes the SWVs recorded at times of 0, 5, and 10 min after the insertion of the microelectrode set into a leaf of *Faucaria tigrina* using a platinum working microelectrode. Upon scanning the potential in the negative direction, the voltammogram is dominated by a prominent cathodic signal at ca. −0.4 V (R_{ox}) which can unambiguously be assigned to the reduction of H_2O_2 eventually superimposed to the reduction of dissolved oxygen [50]. This signal, however, decays rapidly after the insertion of the electrodes thus denoting the apparent rapid exhaustion of the local defense response and the voltammograms display a shoulder at ca. −0.70 V corresponding to the reduction of dissolved oxygen. This behavior differs significantly from that previously reported for *Aloe vera*, where the R_{ox} signal increases progressively until reaching a maximum after ca. 25 min further decreasing slowly [42]. The peak currents measured under our experimental conditions differ slightly but significantly in replicate experiments performed in different leaves of the same plant. This can be attributed to differences in the depth reached by the electrodes in their penetration in the plant leaf and other local variations. For this reason, as discussed below, the peak currents recorded at successive times were normalized relative to the initial peak current in each experiment. This strategy obtained satisfactory repeatability in the normalized peak current/time curves for different specimens of the same species. In turn, significant

differences were obtained in the time evolution of the normalized peak currents recorded for the different studied taxa.

Figure 2 shows the result of a similar mechanical attack now monitored using graphite microelectrodes. This figure shows the SWVs recorded on leaves of a,b) *Crassula ovata* and c,d) *Delosperma cooperi* at intervals of 5 min just after the insertion of the electrodes under two different conditions. Upon scanning the potential scan from 0.00 V vs. Ag/AgCl in the positive direction (Figure 2b,d), there is no electrochemical ROS generation and the voltammograms reflect the "ordinary" plant defense against the stress due to electrode insertion. There is electrochemical ROS generation when the potential is scanned from −0.80 V in the positive direction (Figure 2a,c). According to the literature [52], this is initiated by the one-electron formation of the anion radical superoxide,

$$O_2 + e^- \rightarrow O_2^{\bullet -} \quad (1)$$

This process is followed by a complex sequence of reactions including reaction with water or hydrogenions,

$$O_2^{\bullet -} + H_2O \rightarrow HO_2^{\bullet} + OH^- \quad (2)$$

$$O_2^{\bullet -} + H^+ \rightarrow OH^{\bullet} \quad (3)$$

and/or disproportionation:

$$2O_2^{\bullet -} + H_2O \rightarrow HO_2^- + O_2 + OH^- \quad (4)$$

and/or electrochemical reduction:

$$HO_2^{\bullet}(ads) + e^- \rightarrow HO_2^- \quad (5)$$

ultimately leading to H_2O_2 and H_2O. Different ROS are formed on the electrode surface depending on the experimental conditions [48, 49]. Accordingly, the voltammograms recorded on starting the potential scan at potentials more negative than ca. −0.6 V vs. Ag/AgCl reflect the possibly influence of such ROS species in the defense pathways.

The voltammograms of *Aloe vera* and *Crassula ovata*, as well as those of the Caryophyllales species (*Aptenia cordifolia*, *Delosperma cooperi*, and *Faucaria tigrina*, were similar, being dominated by anodic peaks at ca. 0.85 V (A_1) and ca. 1.2 V (A_2) whose intensity

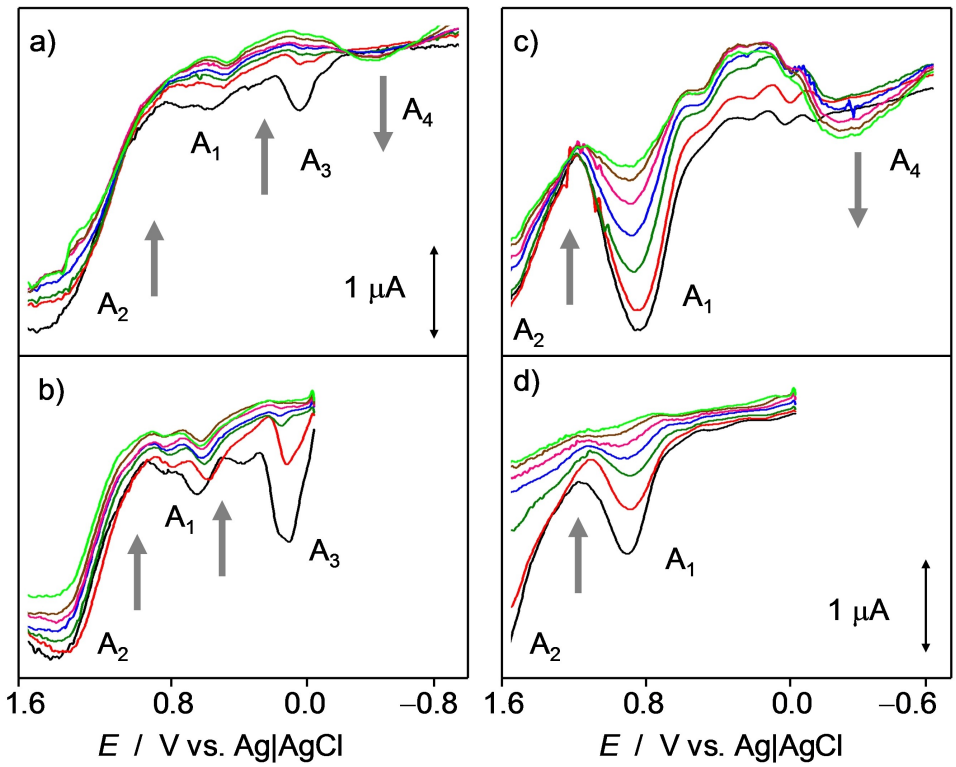

FIGURE 2 SWVs at graphite microelectrode inserted recorded at intervals of 5 min after the insertion of the microelectrode setup on leaves of: a,b) *Crassula ovata* and c,d) *Delosperma cooperi.* Potential scan initiated at: a,c) −0.80 and b,d) 0.00 V vs. Ag/AgCl in the positive direction; potential step increment 4 mV, square wave amplitude 25 mV; frequency 10 Hz. The arrows mark the variation in the intensity of selected peaks in successive voltammograms.

decreased with time both with and without electrochemically generated ROS (see Supplementary Information, Figure S.2). The region between 0.0 and 0.6 V, however, showed significant discrepancies between the different plant species and varied with time for each taxon depending on the presence or not of electrochemically generated ROS. In particular, a peak near 0.0 V (A_3) decreases rapidly with time and disappears when there is electrochemical ROS generation (compare Figures 2a, 2b with Figures 2c, 2d, respectively). In contrast, a signal at ca. −0.3 V (A_4) increases with time.

For our purposes, the relevant point to emphasize is that, although several other electroactive components of plants, flavonoids, lignins, etc. are electrochemically responsive in the 0.0 to 1.2 V region of potentials, the common presence of peaks A_1 and A_2 in all species suggests that these signals can mainly be attributed to the oxidation of SA and JA, respectively [41]. These electrochemical oxidation processes involve the formation of –OH bonds and the release of protons and electrons as schematized in Figure 3.

Accordingly, these signals can be used for the kinetic study of the defense pathway developed in the following section. In turn, the signals between 0.0 and 0.6 V (A_3 in particular) can be assigned to the oxidation of species-characteristic components being eventually responsive to stress. Finally, the signal A_4 can be assigned to a redox process involving a product of degradation generated during the plant defense that is accumulated in the vicinity of the working electrode.

3.2 | SECM imaging

Figure 4 depicts the results of a SECM experiment carried out on a subcuticular thin fragment of *Aloe vera* leave deposited onto a carbon paste bed in contact with 2.5 mM $K_3Fe(CN)_6$ plus 2.5 mM $K_4Fe(CN)_6$ phosphate buffer at pH 7.4 applying to the tip a potential (E_T) of 0.3 V vs. Ag/AgCl when no potential was applied to the substrate ($E_S = 0$). The applied tip potential ensures that the oxidation of $Fe(CN)_6^{4-}$ to $Fe(CN)_6^{3-}$ occurs under diffusion control. Under these conditions, both color plots (a,b) and topographic images (c,d) show a localized deep negative feedback feature corresponding to the thick region of the plant fragment of insulating nature. In freshly cut plant fragments (Figure 2a,c), this is surrounded by positive feedback features which are attributable, in agreement with voltammetric data, to the generation of defense components released in the thinner region of the plant fragment. Since these plant components are oxidizable at the applied tip potential of 0.3 V (see Figure 2), the tip current is enhanced, and this region looks like a more or less peaked positive feedback area. After 10 min, the release of defense components decreases, and the peaked positive feedback features are lowered.

Figure 5 illustrates the results obtained for a similar arrangement when a sequence of different potentials is applied to the substrate. As before (Figure 5a), the freshly cut plant fragment displays a sharp negative feedback feature surrounded by peaked positive feedback. Applying a substrate potential of 1.0 V

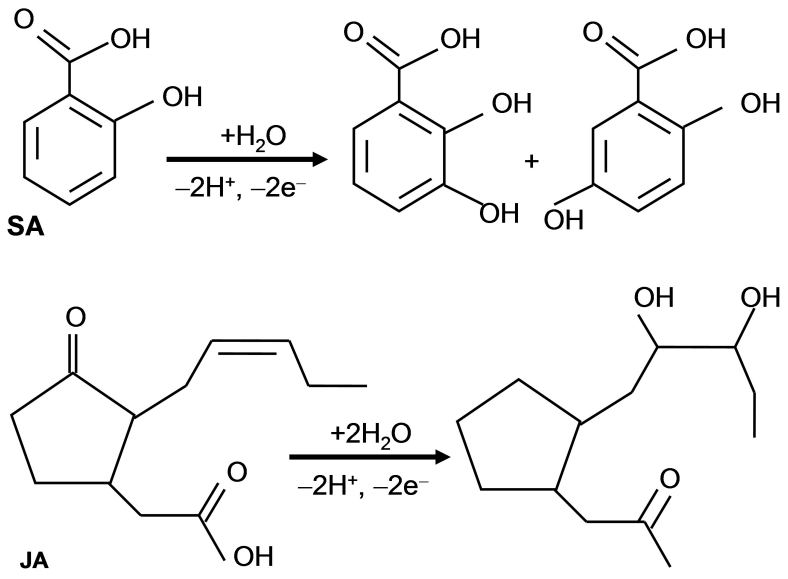

FIGURE 3 Scheme representative of the electrochemical oxidation of salicylic (SA) and jasmonic (JA) acids in aqueous solution.

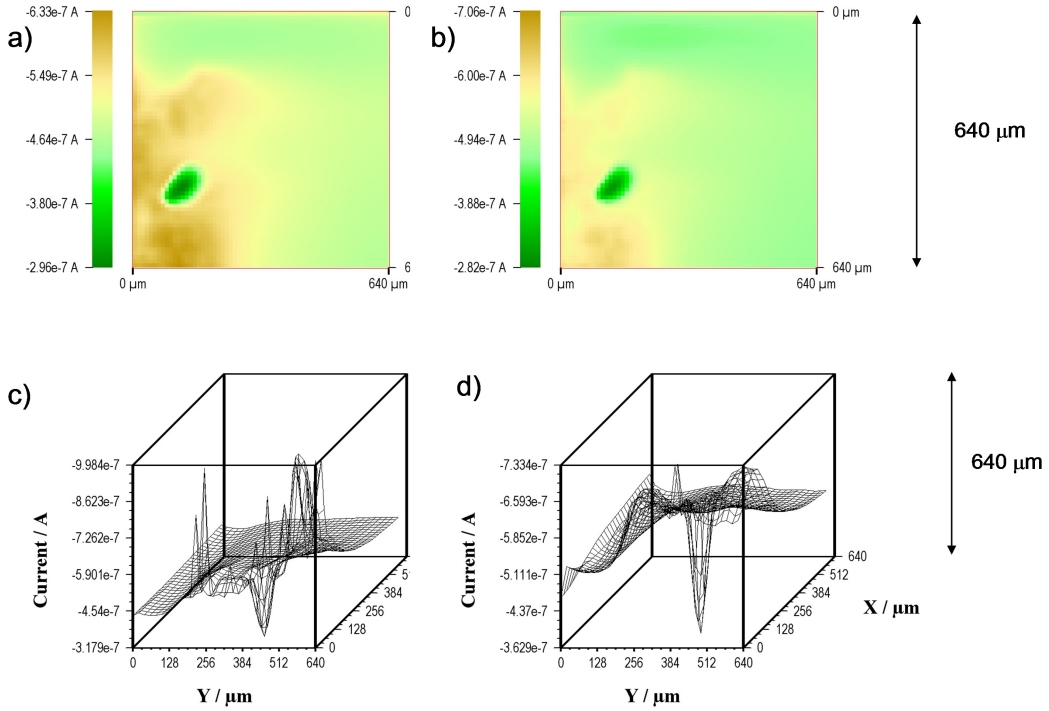

FIGURE 4 a,b) Color plots and c,d) topographic SECM images recorded on a subcuticular fragment of *Aloe vera* leave deposited onto a carbon paste bed in contact with 2.5 mM $K_3Fe(CN)_6$ plus 2.5 mM $K_4Fe(CN)_6$ phosphate buffer at pH 7.4; $E_S = 0$ V; $E_T = 0.3$ V. SECM images of a,c) freshly cut fragment; b,d) the same fragment after 10 min.

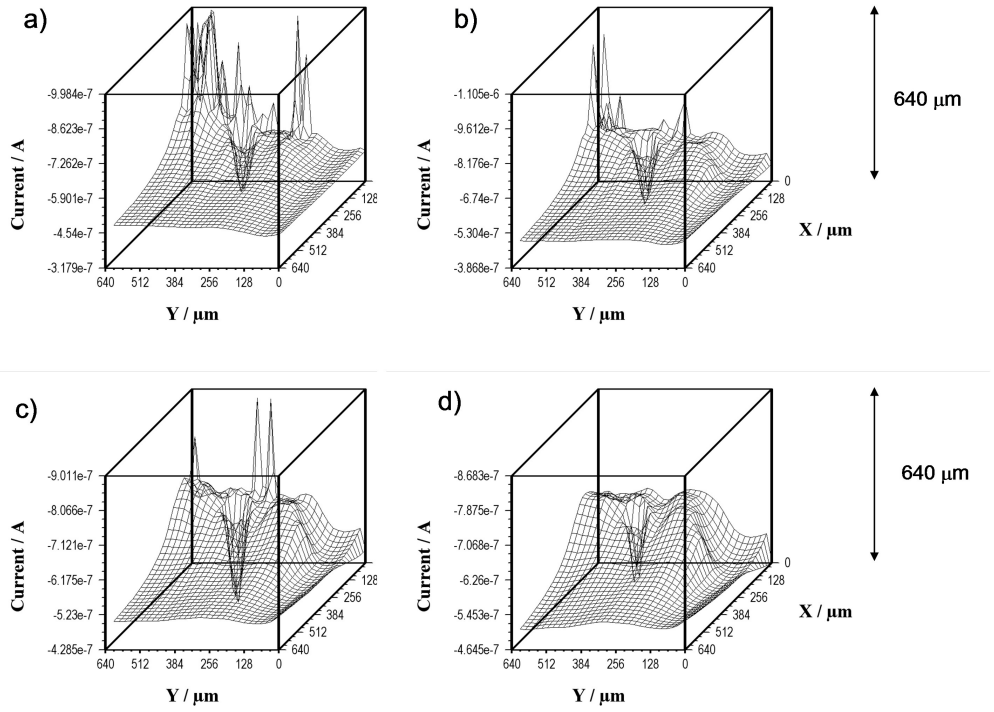

FIGURE 5 Topographic SECM images recorded on a subcuticular fragment of *Aloe vera* leave deposited onto a carbon paste bed in contact with 2.5 mM $K_3Fe(CN)_6$ plus 2.5 mM $K_4Fe(CN)_6$ phosphate buffer at pH 7.4 after the successive application of substrate potentials of a) 0, b) 1.0, c) −0.7, and d) 0 V. $E_T = 0.3$ V.

(Figure 5b), at which the SA and JA can be electrochemically oxidized, the positive feedback features become drastically reduced, as expected as a result of the low process of exhaustion of the defense

response (shown in Figure 2) which adds to the forced consumption of the signaling compounds by the applied potential input. Remarkably, the subsequent application to the substrate of a potential of −0.7 V (Figure 5c) determines the local reactivation of the defense response, evidenced by the new intense positive feedback features appearing in the vicinity of the plant fragment. This can be interpreted as the result of the reactivation of the defense response associated with the electrochemical generation of ROS and their interaction with the plant components. Finally, when the initial conditions ($E_S = 0$) are restored (Figure 5d), the topographic SECM image becomes restricted to the negative feedback feature as observed in Figure 4. Although transport phenomena could influence the SECM imaging, the strong dependence of the topographic features on the potential applied to the substrate suggests that the release of ROS and signaling compounds determine the observed SECM response. Consistently with the literature [53], under several conditions, H_2O_2 can reduce $Fe(CN)_6^{3-}$ to $Fe(CN)_6^{4-}$. Under our experimental conditions, this will produce the local increase of the $Fe(CN)_6^{4-}$ concentration, thus producing an increase of the tip current associated with the electrochemical oxidation of this species.

3.3 | Kinetics of plant defense signaling

Figure 6a compares the variation with time of the ratio between the peak current for H_2O_2 reduction at a time t after the insertion of the electrodes, $I_{ROX}(t)$, and the initial value of this quantity, $I_{ROX}(0)$, for the studied plants determined from voltammetric data in conditions such as in Figure 1. Since the absolute values of $I_{ROX}(t)$ varied slightly in replicate experiments due to minute variations in the depth and location of the electrodes, the $I_{ROX}(t)/I_{ROX}(0)$ ratio was used to normalize data. Absolute values of $I_{ROX}(t)$, are provided as a Supplementary information, Figure S.2. One can see that for *Aloe vera* the $I_{ROX}(t)/I_{ROX}(0)$ ratio varies with time defining approximately a s-shaped curve. This is in contrast with all other species, where this ratio decreases monotonically with time but apparently tends to limit nonzero values for *Crassula ovata* and *Aptenia cordifolia*.

These kinetic patterns can be described, however, using a common generative/degradative kinetics based on the assumptions that: i) the leaves can be approximated to a homogeneous solution; ii) the signaling compound (H_2O_2) is formed from, at least, two different precursors and experiences a subsequent degradation; iii) all the reactions proceed under pseudo-first-order conditions. That can be represented by means of two consecutive reactions (P→A→B; Q→A→B) experienced by two precursor compounds, P, Q, that under stress are activated, yielding A and finally a degradation compound B. According to this scheme, the time variation of the concentrations of P, Q, A and B (c_P, c_Q, c_A, c_B, respectively) will be expressed by the equations:

$$\frac{dc_P}{dt} = -k_P c_P \tag{6}$$

$$\frac{dc_Q}{dt} = -k_Q c_Q \tag{7}$$

$$\frac{dc_A}{dt} = k_P c_P + k_Q c_Q - k_D c_A \tag{8}$$

$$\frac{dc_B}{dt} = k_D c_A \tag{9}$$

Here, k_P, k_Q, k_D, represent the rate constants of the different reactions. In principle, we can assume that all involved compounds are present in leaves in concentrations c°_P, c°_Q, c°_A. Then, integration of Eqs. (6) and (7) leads to:

$$c_P = c_P^o e^{-k_P t} \tag{10}$$

$$c_Q = c_Q^o e^{-k_Q t} \tag{11}$$

Then,

$$\frac{dc_A}{dt} + k_D c_A = k_P c_P^o e^{-k_P t} + k_Q c_Q^o e^{-k_Q t} \tag{12}$$

Multiplying the two terms of the above equation by e^{kDt} leads to:

$$\int_{c_A^o}^{c_A} d\left(c_A e^{k_2 t}\right) = \int_0^t k_1 c_P^o e^{-(k_1 - k_2)t} dt + \int_0^t k_Q c_Q^o e^{-(k_Q - k_2)t} dt \tag{13}$$

The integration of Eq. (13) yields:

$$c_A = c_A^o + \frac{k_P c_P^o}{k_D - k_P}\left[e^{-k_P t} - e^{-k_D t}\right] + \frac{k_Q c_Q^o}{k_D - k_Q}\left[e^{-k_Q t} - e^{-k_D t}\right] \tag{14}$$

When only one precursor (P) operates and $c_A^\circ = 0$, Eq. (14) reduces to the well-known expression for the kinetics of two consecutive reactions:

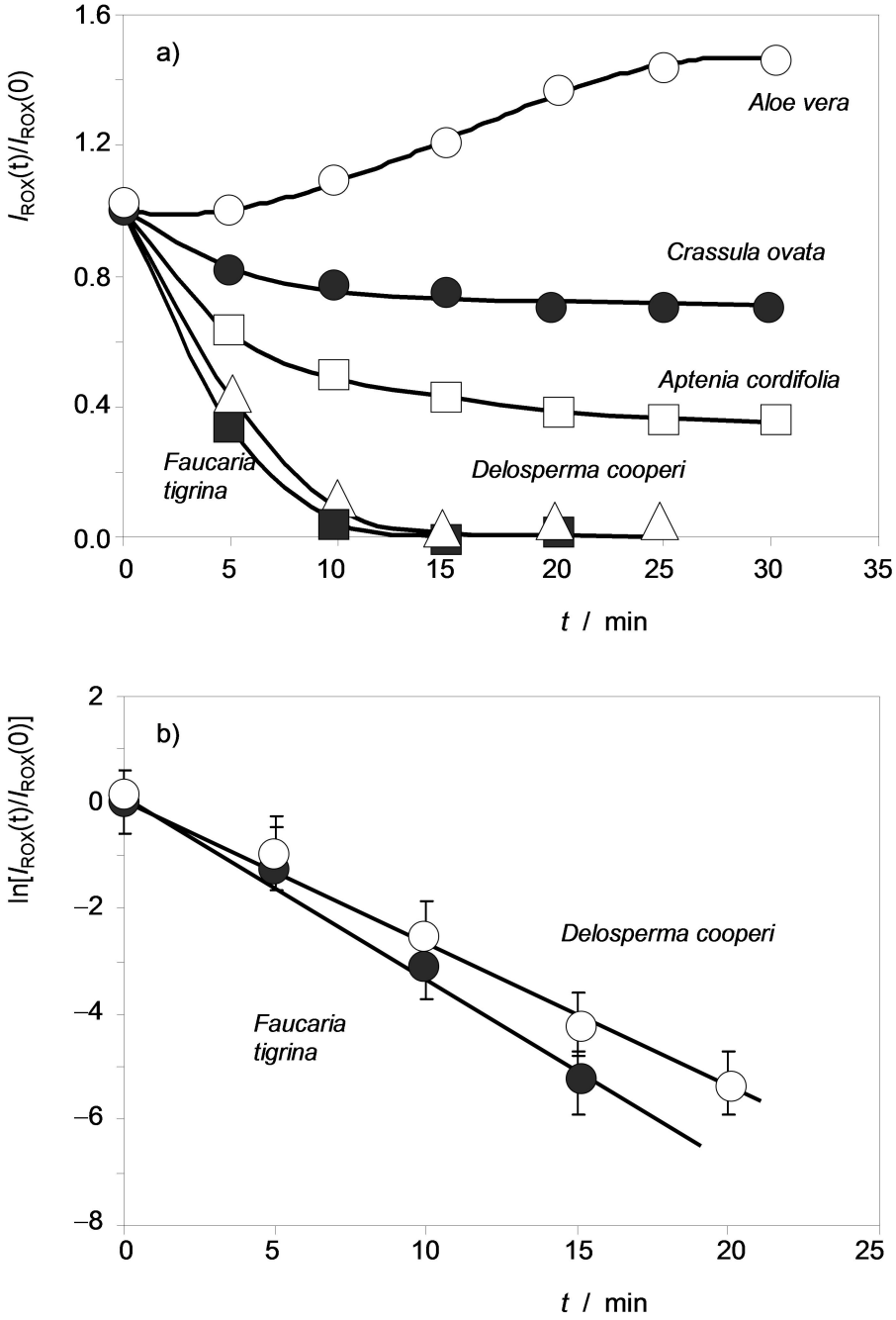

FIGURE 6 a) Variation of the ratio between the peak current for H_2O_2 reduction, $I_{ROX}(t)$, at a time t after the insertion of electrodes and the initial value of this quantity, $I_{ROX}(0)$ with time for plants in this study in voltammograms such as in Figure 1; continuous lines correspond to the theoretical predictions from Eq. (20) taking the rate constant values listed in Table 1. b) Plots of $\ln[I_{ROX}(t)/I_{ROX}(0)]$ vs. time for *Delosperma cooperi*, and *Faucaria tigrina*. Averaged values from three replicate measurements. Error bars omitted for clarity in (a).

$$c_A = \frac{k_P c_P^o}{k_D - k_P}\left[e^{-k_P t} - e^{-k_D t}\right] \quad (15)$$

At time zero, c_A is given by:

$$c_A \approx c_A^o + \frac{k_Q c_Q^o}{k_D} \quad (16)$$

A case of particular interest is when $k_D \gg k_Q$. Then, Eq. (14) reduces to:

$$c_A \approx c_A^o + \frac{k_P c_P^o}{k_D - k_P}\left[e^{-k_P t} - e^{-k_D t}\right] + \frac{k_Q c_Q^o}{k_D} e^{-k_Q t} \quad (17)$$

The above equations can directly be correlated with experimental voltammetric data assuming that peak

currents ($I(t)$) measured for the voltammetric peak characteristic of the signaling compound A are proportional to the concentration of this species. Introducing an electrochemical constant, g, Eqs. (14) and (17) can be rewritten as:

$$I(t) = gc_A^o + g\frac{k_P c_P^o}{k_D - k_P}\left[e^{-k_P t} - e^{-k_D t}\right] + g\frac{k_Q c_Q^o}{k_D - k_Q}\left[e^{-k_Q t} - e^{-k_D t}\right] \quad (18)$$

$$I(t) \approx gc_A^o + g\frac{k_P c_P^o}{k_D - k_P}\left[e^{-k_P t} - e^{-k_D t}\right] + g\frac{k_Q c_Q^o}{k_D}e^{-k_Q t} \quad (19)$$

To compare the results for different plants avoiding the effect of the electrochemical constant, it is convenient to use the ratio between the current measured at a time t, $I(t)$, and the current at time zero, $I(0)$, i. e.:

$$\frac{I(t)}{I(0)} \approx \frac{c_A^o + \frac{k_P c_P^o}{k_D - k_P}\left[e^{-k_P t} - e^{-k_D t}\right] + \frac{k_Q c_Q^o}{k_D}e^{-k_Q t}}{c_A^o + (k_Q/k_P)c_Q^o} \quad (20)$$

When k_P and k_D are quite similar, Eq. (20) tends to convert into an exponential decay given by:

$$\frac{I(t)}{I(0)} \approx \frac{1}{c_A^o + (k_Q/k_P)c_Q^o}\left(c_A^o + \frac{k_Q c_Q^o}{k_D}e^{-k_Q t}\right) \quad (21)$$

Experimental $I_{ROX}(t)/I_{ROX}(0)$ data for *Aloe vera*, *Crassula ovata* and *Aptenia cordifolia* can be satisfactorily fitted to Eq. (20) taking the rate constant values listed in Table 1. The resulting theoretical values are depicted as continuous lines in Figure 6a. In the case of *Delosperma cooperi* and *Faucaria tigrina* experimental data can be fitted to Eq. (21) resulting in linear $\ln[I_{ROX}(t)/I_{ROX}(0)]$ vs. $\ln t$ representations (see Figure 6b). From these linear plots, we obtain first-order rate constants of $0.28 \pm 0.02\ min^{-1}$ for *Delosperma cooperi*, and $0.35 \pm 0.04\ min^{-1}$ for *Faucaria tigrina*.

3.4 | Kinetics of salicylic acid and jasmonic acid pathways

As previously discussed, the time variation of the concentration of SA and JA can be represented by the variation of the peak current for the oxidation processes A_1, $I_{A1}(t)$, and A_2, $I_{A2}(t)$, respectively. As before, replicate experiments are normalized taking the ratio between the peak current recorded at a time t after the insertion of the electrodes and the initial value of this quantity ($I_{A1}(0)$, $I_{A2}(0)$, respectively). Figure 7 shows the time variation of experimental values of the $I_{A1}(t)/I_{A1}(0)$ ratio for plants in this study from data recorded in voltammograms such as in Figure 2 in conditions of no ROS generation. These experimental data, representative of the evolution of the concentration of SA, can also be fitted to the precedent generation/decomposition model. In this figure, the continuous lines correspond to the theoretical predictions from Eq. (20) taking the rate constant values listed in Table 2.

Interestingly, the variation of the $I_{A2}(t)/I_{A2}(0)$ with time, representative of the production of JA under stress, can be described in terms of the aforementioned model. The corresponding rate constants recorded in conditions of no ROS generation are summarized in Table 2.

The kinetic model is also applied under conditions of electrochemical ROS generation. However, there are remarkable differences between the different plants when the peak current/time curves recorded with and without electrochemical ROS generation are compared. Figure S.3 (Supplementary information) depicts the plots of: a–c) $I_{A1}(t)/I_{A1}(0)$vs. time, and d–f) the

TABLE 1 Kinetic parameters determined from H_2O_2 reduction peak recorded at Pt microelectrodes in conditions such as in Figure 1. n.d.: non-determined.

Plant	k_Q (min^{-1})	k_P (min^{-1})	k_D (min^{-1})
Aloe vera	0.09 ± 0.01	0.0015 ± 0.002	0.20 ± 0.03
Asphodelus fistulosus	0.20 ± 0.03	0.010 ± 0.002	0.20 ± 0.03
Bulbine frutescens	0.12 ± 0.03	0.008 ± 0.002	0.22 ± 0.03
Crassula ovata	0.17 ± 0.02	0.0020 ± 0.003	0.21 ± 0.03
Graptopetalum paraguayense	0.14 ± 0.02	0.0015 ± 0.002	0.09 ± 0.02
Sedum sediforme	0.14 ± 0.02	0.0020 ± 0.003	0.11 ± 0.02
Aptenia cordifolia	0.18 ± 0.01	0.0019 ± 0.002	0.20 ± 0.03
Delosperma cooperi	0.28 ± 0.02	n.d.	n.d.
Faucaria tigrina	0.35 ± 0.04	n.d.	n.d.

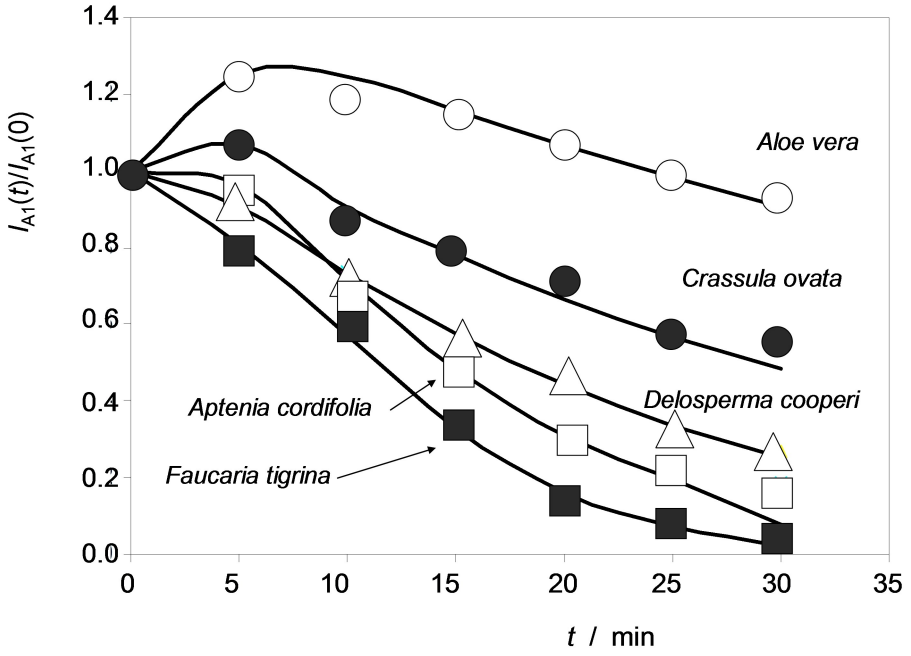

FIGURE 7 Variation of the $I_{A1}(t)/I_{A1}(0)$ ratio, representative of the concentration of SA, with time for plants in this study. Data from voltammograms recorded such as in Figure 2 in conditions of no ROS generation. Continuous lines correspond to the theoretical predictions from Eq. (20) taking the rate constant values listed in Table 2.

TABLE 2 Kinetic parameters determined from SA oxidation peak (A_1) and JA oxidation peak (A_2) recorded under conditions of no electrochemical ROS generation at graphite microelectrodes in conditions such as in Figure 2.

A_1 (SA)	**k_Q (min^{-1})**	**k_P (min^{-1})**	**k_D (min^{-1})**
Aloe vera	0.020 ± 0.003	0.040 ± 0.002	0.30 ± 0.02
Asphodelus fistulosus	0.040 ± 0.003	0.030 ± 0.003	0.30 ± 0.02
Bulbine frutescens	0.020 ± 0.003	0.030 ± 0.003	0.30 ± 0.02
Crassula ovata	0.030 ± 0.003	0.041 ± 0.002	0.35 ± 0.02
Graptopetalum paraguayense	0.008 ± 0.0003	0.012 ± 0.003	0.20 ± 0.03
Sedum sediforme	0.015 ± 0.003	0.024 ± 0.004	0.25 ± 0.02
Aptenia cordifolia	0.10 ± 0.03	0.080 ± 0.006	0.10 ± 0.02
Delosperma cooperi	0.20 ± 0.03	0.050 ± 0.004	0.06 ± 0.01
Faucaria tigrina	0.22 ± 0.03	0.048 ± 0.004	0.06 ± 0.01
A_2 (JA)	**k_Q (min^{-1})**	**k_P (min^{-1})**	**k_D (min^{-1})**
Aloe vera	0.025 ± 0.003	0.040 ± 0.004	0.05 ± 0.02
Asphodelus fistulosus	0.023 ± 0.003	0.035 ± 0.003	0.06 ± 0.02
Bulbine frutescens	0.025 ± 0.003	0.030 ± 0.003	0.08 ± 0.02
Crassula ovata	0.010 ± 0.003	0.060 ± 0.004	0.30 ± 0.04
Graptopetalum paraguayense	0.020 ± 0.003	0.040 ± 0.004	0.25 ± 0.04
Sedum sediforme	0.020 ± 0.003	0.040 ± 0.004	0.30 ± 0.04
Aptenia cordifolia	0.022 ± 0.004	0.055 ± 0.004	0.15 ± 0.03
Delosperma cooperi	0.020 ± 0.003	0.050 ± 0.004	0.15 ± 0.03
Faucaria tigrina	0.019 ± 0.003	0.050 ± 0.004	0.14 ± 0.03

$I_{A2}(t)/I_{A2}(0)$ vs. time superimposing the data recorded under conditions of no ROS generation (circles) and electrochemical ROS generation (solid circles) for a,d) *Aloe vera*, b,e) *Crassula ovata* and c,f) *Delosperma cooperi*. Experimental data for the other tested species revealed a significant homogeneity in the results

obtained for the plants of the same family. The values of the rate constants determined in conditions of ROS generation are listed in Tables S.1 and S.2 of Supplementary information.

Examination of data in Table 2 and Tables S.1 and S.2 reveals that in the case of SA, there are few differences in the kinetic parameters recorded in the absence and in the presence of electrochemically generated ROS. That can be interpreted as assuming that the SA signaling pathway is scarcely responsive to ROS under our experimental conditions. This feature, however, is particularly significant in the case of the Caryophyllales, where there is no difference between the $I_{A1}(t)/I_{A1}(0)$ vs. time curves recorded in the absence and in the presence of electrochemically generated ROS.

Consistently, the plots of the $I_{A1}(t)/I_{A1}(0)$ ratio measured under conditions of no ROS generation, vs. the same $I_{A1}(t)/I_{A1}(0)$ ratio measured under conditions of electrochemical ROS generation for *Crassula ovata*, *Delosperma cooperi*, *Aptenia cordifolia* and *Faucaria tigrina* fit well to a straight line by the origin and slope close to one, as can be seen in Figure 8. This essentially common representation suggests that electrochemically generated ROS does not influence the defense response associated to SA under our experimental conditions. For *Aloe vera* and *Crassula ovata*, however, the forced linear fit of experimental data leads to clearly different paths. In contrast, rate constants in Table 2 denotes that the presence of electrochemically generated ROS alters significantly the kinetics of the JA signaling pathway.

3.5 | Discussion

The experimental arrangement used here involves applying electrochemical inputs combined with mechanical aggression to the epithelial and sub-epithelial regions of the plant leaves under aerobic conditions. This implies that, strictly, mechanical stress associated with the penetration of the electrodes into the vegetal tissues is superimposed on electrical stimulation. It will be assumed that both effects are largely confined to a small region near the electrodes and that the main electrical effect is the generation of ROS when the potential is cathodic enough to produce the reduction of dissolved oxygen. As noted in the Introduction section, there are a number of other than phylogenetic factors influencing the plant defense response. Then, the approach reported here must be taken with caution regarding its phylogenetic implications. Under this critical view, the previous results can be summarized as:

a) The kinetics of both SA and JA, as well as that of H_2O_2, can be satisfactorily described in terms of two competing pseudo-first-order generation reactions. The signaling compounds are produced from two precursor compounds, P, Q, through two competing pathways (P-path and Q-path) with rate constants k_P,

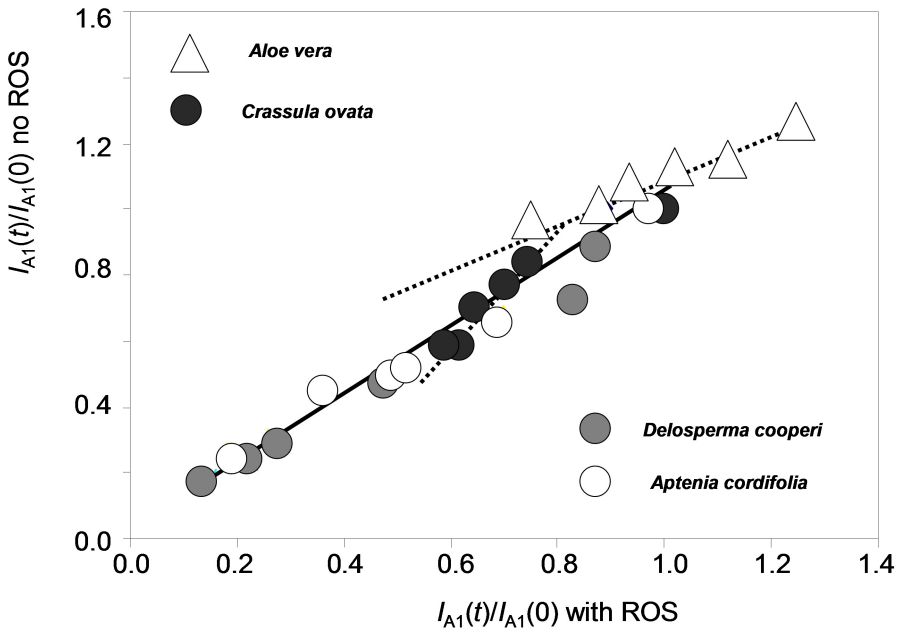

FIGURE 8 Variation of the $I_{A1}(t)/I_{A1}(0)$ ratio measured in voltammograms such as in Figure 2b,d in conditions of no ROS generation with the same ratio measured in conditions of ROS generation (Figure 2a,c) for plants in this study grouped by orders. The represented peak current ratio is representative of the concentration of SA.

k_Q. These processes are followed by a first-order degradation process (rate constant k_D).

b) The rate constants depend on the plant species and are also dependent on the presence of electrochemically generated ROS. The kinetic parameters are clearly homogeneous within each one of the studied orders.

For our purposes, it is interesting to investigate the possible coupling between SA, JA and H_2O_2 production under stress. Our data depict a more complex scenario than that described in our previous study on *Aloe vera* [42]. The relevant point to emphasize is that the behavior of the different plants is reflected in differences between the 'fast' generation pathway (Q-path, defined by k_Q) and the 'slow' generation pathway (P-path, defined by k_P).

Our data suggest that SA and JA pathways are coupled with respect to the 'slow' P-path, as can be seen in Figure 9, where the rate constant values of JA (k_P-(JA) are plotted vs. the corresponding values for SA (k_P(SA)). Here, the data points (Table 2) for the plants of the different families fall in well-defined straight lines passing by the origin, thus suggesting that the corresponding P-pathways for SA and JA are coupled.

Figure 10a shows the plots of the k_Q values for SA vs. the k_Q values for H_2O_2 (respectively, k_Q(SA) and k_Q-(H_2O_2), using data summarized in Tables 1 and 2 for plants in this study. These rate constants are representative of the 'fast' (Q-path) generation path of the respective signaling compound. Again, the Caryophyllales define a straight line passing by the origin. In contrast, the k_Q(SA) values of Asparagales and Saxyfragales appear to less clearly dependent of the corresponding k_Q(H_2O_2) ones. These data suggest that the 'fast' generation step of SA and H_2O_2 are decoupled for the Asparagales and Saxyfragales and coupled for Caryophyllales. The decoupling between H_2O_2 generation and JA in the 'fast' Q-path is extended to all three orders, as can be seen in Figure 10b, where k_Q(JA) is plotted vs. k_Q(H_2O_2).

On comparing the k_Q values for SA and JA determined with and without electrochemical ROS generation, one can see that these values appear only coupled for the Caryophyllales species (see data in Tables 1, 2, S.1, S.2, and S.3). That suggests that the coupling of the Q-pathway for both SA and JA occurred at any evolutionary stage during preceding the separation of the Caryophyllales. These results can also be interpreted in regard to plant phylogeny. It is pertinent to underline that depending on the availability of the fossil record, a significant portion of the information on their phylogenetic relationships must come from considering the living members of these taxonomic groups. Accordingly, the phylogeny of these groups is a matter of speculation to some extent [44–47]. In principle, the origin of these taxa can be associated with successive rapid evolutionary

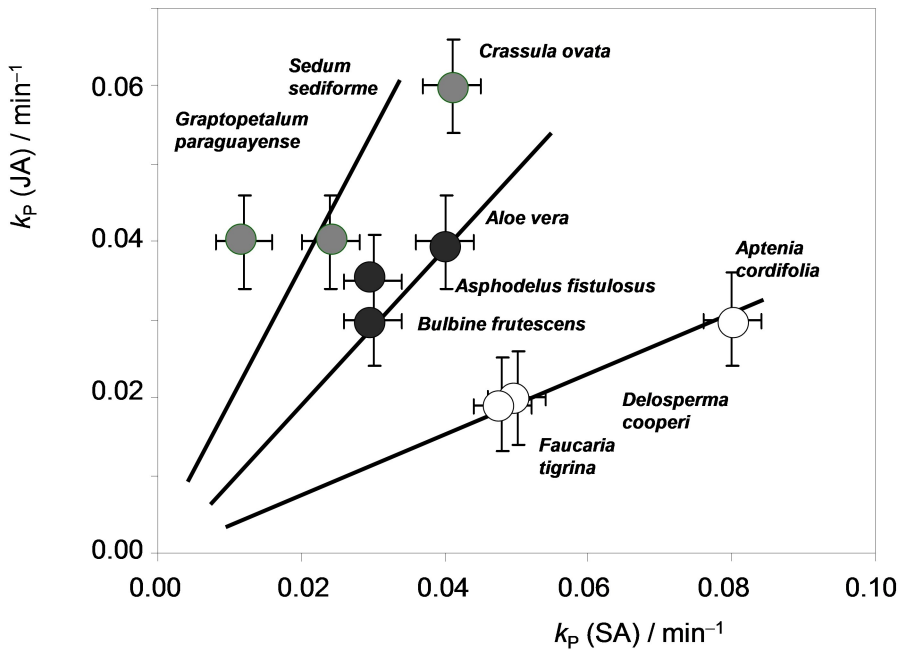

FIGURE 9 Plots of k_P(JA) vs. k_P(SA) for plants in this study grouped by orders. These parameters correspond to the rate constants of the 'slow' generative step (P-path) of the respective signaling compound from their precursors in plants. From rate constant values in Tables 1 and 2.

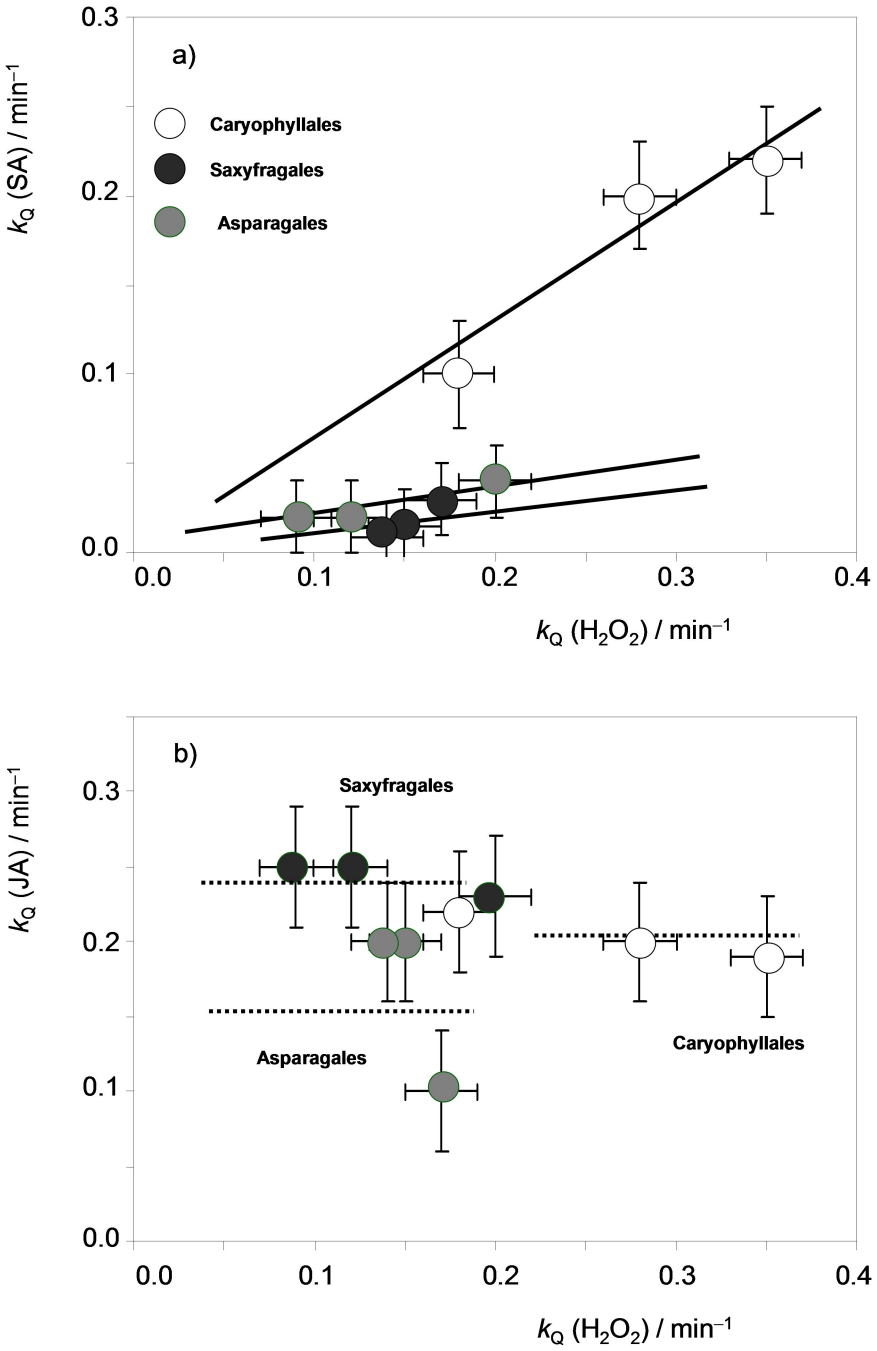

FIGURE 10 Plots of: a) k_Q(SA) vs. $k_Q(H_2O_2)$, and b) k_Q(JA) vs. $k_Q(H_2O_2)$ for plants in this study grouped by families. These parameters correspond to the rate constants of the 'fast' generative step (Q-path) of the respective signaling compound from their precursors in plants. From rate constant values in Tables 1 and 2.

radiations initiated around 115 Ma [54]. Although the genetic information of contemporary species focuses on the phylogenetic debate, chemical information is also of significant interest. In particular, it has been established that a part of Caryophyllales synthesize betalains pigments while other species of the same order synthesize anthocyanins and these two types of pigments are mutually excluded [55].

Our kinetic data are potentially interesting concerning phylogenetics. The essential idea is that changes in plant physiology should accompany genetic changes determining the evolutionary ramifications of taxa. These physiological changes could affect, among others, the defense system(s) so that it is conceivable that the phylogenetic ramifications were accompanied by sharp changes in the defense system and that these

changes were retained by the successors of the primitive species.

Our data suggest that there are at least two disruptions in the plant response to stress: i) the decoupling of SA and H_2O_2 Q-pathways, and ii) the no sensitivity of the Q-path of SA and JA generation to 'free' ROS. These are superimposed on a simplified phylogenetic tree in Figure 11. One of the possible scenarios derived from the data reported here can be summarized as two hypotheses: i) the separation between monocots and eudicots could involve the decoupling of the 'fast' Q-response to stress due to SA and H_2O_2; ii) the separation of the Caryophyllales from other eudicots would be associated to the lost of ROS sensitivity in the Q-type SA response pathway.

Despite their hypothetical nature, the foregoing set of considerations supports the idea that electrochemistry can be used as an analytical tool complementing biochemical and genetic research in order to provide information of interest in the phylogenetic domain [39, 56], necessarily being complemented by studies incorporating genetic and epigenetic considerations.

4 | CONCLUSIONS

The time variation of the *in situ* voltammetric signals associated to H_2O_2 reduction and the oxidation of SA and JA, recorded upon insertion of microelectrodes into the leaves of different plants, reflects the kinetics of their defense response against stress. The voltammetric response of three species of the orders Asparagales (*Aloe vera*, *Asphodelus fistulosus*, and *Bulbine frutescens*), Caryophyllales (*Aptenia cordifolia*, *Delosperma cooperi*, and *Faucaria tigrina*), and Saxifragales (*Crassula ovata*, *Sedum sediforme*, and *Graptopetalus paraguayense*) exhibits common patterns at this taxonomic level.

The peak current vs. time curves can satisfactorily be fitted to a common kinetic model based on two competing generation reactions accompanied by a degradation process, all involving pseudo-first-order conditions. The kinetics is sensitive to the electrochemical generation of ROS the rate constants being homogeneous at the order level.

Correlation between kinetic parameters suggests different coupling/decoupling between the SA and JA signaling/defense response pathways and H_2O_2 production in the studied orders. It is hypothesized that these differences can reflect different evolutionary pathways of the studied taxa. Reported data suggest that the separation between monocots and eudicots and the subsequent separation of the Caryophyllales from other eudicots could be associated to changes in the signaling pathways. Accordingly, the kinetic analysis of the reported electrochemical methodology can be potentially usable to establish phylogenetic and evolutionary relationships complementing well-established genetic studies.

AUTHOR CONTRIBUTION

ADC conceptualized, analyzed data and drafted the paper, DD and NM performed electrochemical

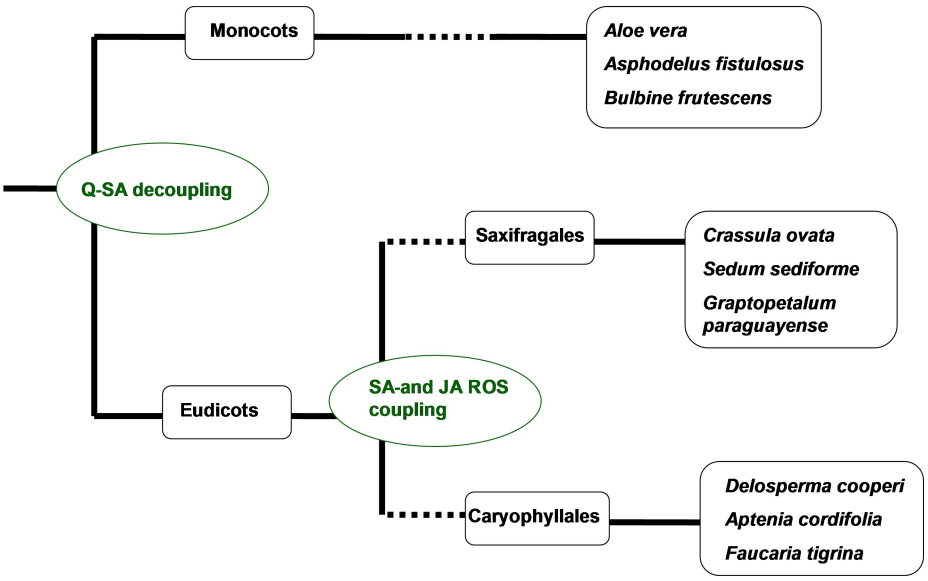

FIGURE 11 Hypothetical decoupling steps associated to the phylogenetic evolution of the studied orders.

experiments and processed quantitative data; JP-M provided plant specimens and revised botanic aspects.

ACKNOWLEDGMENTS

Grant PID2020-113022GB-I00 funded by MCIN/AEI/10.13039/501100011033 and by "ERDF A way of making Europe", by the "European Union frame is gratefully acknowledged.

CONFLICT OF INTEREST STATEMENT

The authors declare no conflict of interest.

DATA AVAILABILITY STATEMENT

Data are available on request to the authors.

ORCID

Daiane Dias http://orcid.org/0000-0002-4057-2471

REFERENCES

1. P. Bianco, M. Aghroud, *Electroanalysis* **1997**, *9*, 602.
2. P. Ciosek, B. Pokorska, E. Romanoswska, W. Wróbléwski, *Electroanalysis* **2006**, *18*, 1266.
3. J. Church, S. M. Armas, P. K. Patel, K. Chumbimuni-Torres, W. H. Lee, *Electroanalysis* **2018**, *30*, 626.
4. C. Wasternack, B. Hause, *Ann. Bot.* **2013**, *111*, 1058.
5. M. Erb, S. Meldau, I. T. Baldwin, *Ann. Bot.* **2012**, *110*, 1503.
6. M. Heil, *Trends Plant Sci.* **2009**, *14*, 356.
7. J.-Y. Zhou, X. Li, D. Zhao, M.-Y. Deng-Wang, C.-C. Dai, *Planta* **2016**, *244*, 699.
8. F. Shaki, H. E. Maboud, V. Miknam, *Curr. Plant Biol.* **2018**, *13*, 16.
9. K. Sueda, K. Nanya, I. Uyeda, Y. Tasaka, R. Ogura, K. Hiratsuka, T. Matsumura, *Curr. Plant Biol.* **2022**, *30*, 100245.
10. C. Wasternack, *Ann. Bot. (London)* **2007**, *100*, 681.
11. A. A. Agrawal, *Funct. Ecol.* **2011**, *25*, 420.
12. C. L. Ballaré, *Trends Plant Sci.* **2011**, *16*, 249.
13. A. Koornneef, A. Leon-Reyes, T. Ritsema, A. Verhage, F. C. Den Otter, L. C. Van Loon, C. M. J. Pietersen, *Plant Physiol.* **2008**, *147*, 1358.
14. K. Kawazu, A. Mochizuki, Y. Sato, W. Sugeno, M. Murata, S. Seo, I. Mitsuhara, *Arthropod-Plant Interact.* **2012**, *6*, 221.
15. J. P. Anderson, E. Badruzsaufari, P. M. Schenk, J. M. Manners, O. J. Desmond, C. Ehlert, D. J. Maclean, P. R. Ebert, K. Kazan, *Plant Cell* **2004**, *16*, 3460.
16. D. Chen, C. R. M. Wilkinson, S. Watt, C. J. Penkett, W. M. Toone, N. Jones, J. Bahler, *Mol. Biol. Cell* **2008**, *19*, 308.
17. M. D. Bolton, *Plant Microbe Interact.* **2009**, *22*, 487.
18. C. C. Labandeira, *Annu. Rev. Ecol. Syst.* **1997**, *28*, 153.
19. K. J. Niklas, B. H. Tiffney, A. H. Knoll, in *Phanerozoic Diversity Patterns: Profiles in Macroevolution*, J. W. Valentine, Ed.; Princeton University Press: Princeton, NJ, USA, **1985**; pp. 97–128.
20. J. Schönenberger, E. M. Friis, M. L. Matthews, P. K. Endress, *Ann. Bot.* **2001**, *88*, 423.
21. J. Fürstenberg-Hägg, M. Zagrobelny, S. Bak, *Int. J. Mol. Sci.* **2013**, *14*, 10242.
22. Z. Alijbori, M. S. Chen, *Insect Sci.* **2018**, *25*, 2.
23. M. Fujita, Y. Fujita, Y. Noutoshi, F. Takahashi, Y. Narusaka, K. Yamaguchi-Shinozaki, K. Shinozaki, *Curr. Opin. Plant Biol.* **2006**, *9*, 436.
24. S. Fraire-Velázquez, R. Rodríguez-Guerra, L. Sánchez-Calderón, Abiotic and Biotic Stress Response Crosstalk in Plants, in *Abiotic Stress Response in Plants–Physiological, Biochemical and Genetic Perspectives*; A. Shanker, Ed.; InTech: Rijeka, **2011**; p. 346.
25. A. Mhamdi, F. Van Breusegem, *Development* **2018**, *145*, 164376.
26. R. Mittler, *Trends Plant Sci.* **2016**, *16*, 300.
27. G. Noctor, C. H. Foyer, *Plant Physiol.* **2017**, *171*, 1591.
28. M. J. Merati, H. Hassanpour, V. Niknam, M. Mirmasoumi, *J. Plant Interact.* **2014**, *9*, 791.
29. F. Palma, C. Lluch, C. Iribarne, J. M. García-Garrido, N. A. T. García, *Plant Growth Regul.* **2009**, *58*, 307.
30. M. Sorahinobar, V. Niknam, H. Ebrahimzadeh, H. Soltanloo, M. Behmanesh, S. T. Enferadi, *J. Plant Growth Regul.* **2016**, *35*, 477.
31. M. Hilgemann, F. Scholz, H. Kahlert, L. M. de Carvalho, M. Barcellos da Rosa, U. Lindequist, M. Wurster, P. C. do Nascimento, D. Bohrer, *Electroanalysis* **2010**, *22*, 406.
32. T. Xu, N. Scafa, L.-P. Xu, L. Su, C. Li, S. Zhou, Y. Liu, X. Zhang, *Electroanalysis* **2014**, *26*, 449.
33. A. K. Yagati, J.-W. Choi, *Electroanalysis* **2014**, *26*, 1259.
34. N. I. Ismail, S. Sornambikai, M. R. A. Kadir, N. H. Mahmood, R. M. Zulkifli, S. Shahir, *Electroanalysis* **2018**, *30*, 2939.
35. Q.-Q. Ren, X.-R. Huang, G.-C. Liu, O.-Y. Jun, M.-T. Li, H. Chen, Y.-D. Zhao, W. Chen, *Sens. Actuators B* **2015**, *220*, 743.
36. F. Ai, H. Chen, S.-H. Zhang, S.-Y. Liu, F. Wei, X. Y. Dong, J.-K. Cheng, W.-H. Huang, *Anal. Chem.* **2009**, *81*, 8453.
37. A. Doménech-Carbó, N. Montoya, P. Soriano, E. Estrelles, *Curr. Plant Biol.* **2018**, *16*, 9.
38. A. Doménech-Carbó, G. Cebrián Torrejón, A. Lopes-Souto, M. Martins de Moraes, M. Jorge-Kato, J. Fechine-Tavares, J. M. Barbosa-Filho, *RSC Adv.* **2015**, *5*, 61006.
39. A. Doménech-Carbó, A. M. Ibars, J. Prieto-Mossi, E. Estrelles, F. Scholz, G. Cebrián-Torrejón, M. Martini, *New J. Chem.* **2015**, *39*, 7421.
40. A. Doménech-Carbó, A. M. Ibars, J. Prieto-Mossi, E. Estrelles, M. T. Doménech-Carbó, A. S. Ortiz-Miranda, Y. Lee, *Electroanalysis* **2017**, *29*, 643.
41. E. M. Mateo, J. V. Gómez, N. Montoya, R. Mateo-Castro, J. V. Gimeno-Adelantado, M. Jiménez, A. Doménech-Carbó, *Food Chem.* **2018**, *267*, 91.
42. A. Doménech-Carbó, D. Dias, M. Donnici, *Electroanalysis* **2021**, *33*, 1024.
43. APG III (The angiosperm phylogeny group), *Bot. J. Linn. Soc.* **2009**, *161*, 105.
44. P. Cuénoud, V. Savolainen, L. W. Chatrou, M. Powell, R. J. Grayer, M. W. Chase, *Am. J. Bot.* **2002**, *89*, 132.
45. M. Fishbein, D. E. Soltis, *System. Bot.* **2004**, *29*, 883.

46. D. E. Soltis, M. E. Mort, M. Latvis, E. V. Mavrodiev, B. C. O'Meara, P. S. Soltis, J. Gordon Burleigh, R. Rubio de Casas, *Am. J. Bot.* **2013**, *100*, 916.
47. O. Seberg, G. Petersen, J. I. Davis, J. Chris Pires, D. W. Stevenson, M. W. Chase, M. F. Fay, D. S. Devey, T. Jørgensen, K. J. Sytsma, Y. Pillon, *Am. J. Bot.* **2012**, *99*, 875.
48. T. A. Enache, A. M. Chiorcea-Paquim, O. Fatibello-Filho, A. M. Oliveira-Brett, *Electrochem. Commun.* **2009**, *11*, 1342.
49. A. Kapałka, G. Foti, C. Comninellis, *Electrochim. Acta* **2009**, *54*, 2018.
50. A. Doménech-Carbó, R. Gavara, P. Hernández, I. Domínguez, *Talanta* **2015**, *144*, 1207.
51. K. Karnicka, K. Eckhard, D. A. Guschin, L. Stoica, P. J. Kulesza, W. Schumann, *Electrochem. Commun.* **2007**, *9*, 1998.
52. J. Xu, W. Huang, R. L. McCreery, *J. Electroanal. Chem.* **1996**, *410*, 235.
53. A. Katafias, O. Impert, *Transition Met. Chem.* **2008**, *33*, 1041.
54. O. Seberg, G. Petersen, J. I. Davis, J. Chris Pires, D. W. Stevenson, M. W. Chase, M. F. Fay, D. S. Devey, T. Jørgensen, K. J. Sytsma, Y. Pillon, *Am. J. Bot.* **2012**, *99*, 875.
55. S. F. Brockington, R. H. Walker, B. J. Glower, P. S. Soltis, D. E. Soltis, *New Phytol.* **2011**, *190*, 854.
56. A. Doménech-Carbó, Electrochemistry of plants: basic theoretical research and applications in plant science, *J. Solid State Electrochem.* **2021**, *25*, 2747.

SUPPORTING INFORMATION

Additional supporting information can be found online in the Supporting Information section at the end of this article.

How to cite this article: A. Doménech-Carbó, D. Dias, J. Prieto-Mossi, N. Montoya, *Electroanalysis* **2023**, *35*, e202300087. https://doi.org/10.1002/elan.202300087